RealD²iff:

Bridging Real-World Gap in Robot Manipulation via Depth Diffusion

Xiujian Liang 1,2 , Jiacheng Liu 1,3,5 , Mingyang Sun 1,3,5 , Qichen He 1,4 , Cewu Lu 1,4 , Jianhua Sun 1,4† SII, 2 FDU, 3 WU, 4 SJTU, 5 ZJU

liangxj23@m.fudan.edu.cn, gothic@sjtu.edu.cn

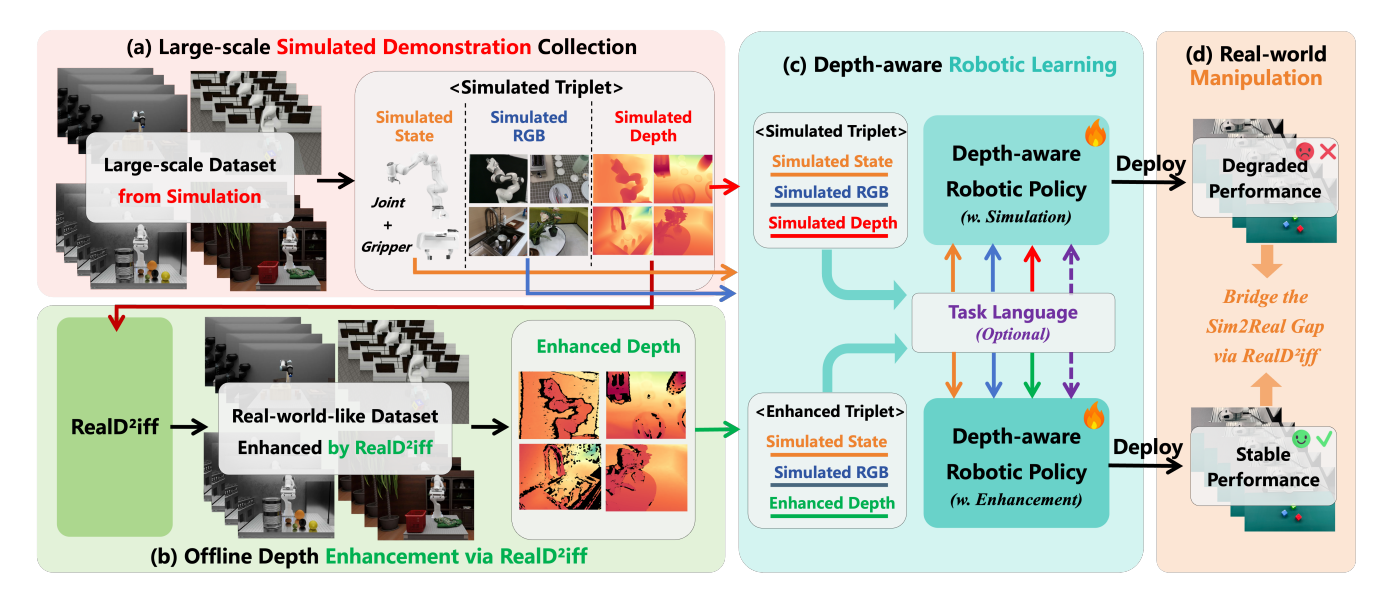


Figure 1. How the proposed RealD2iff makes real-world-like robot learning in simulation. (a) Large-scale dataset of diverse demonstrations is collected in a simulation, including states of joint and gripper, RGB images and depth data. (b) Depth data is enhanced offline using the RealD2iff, which generates real-world-like noisy depth. (c) The simulated or enhanced data is fed into depth-aware robotic policies for learning, with task instruction optional as language data. (d) The trained policies are deployed in real-world robot manipulation, showing the effectiveness of RealD2iff in enabling zero-shot sim2real transfer, with stable task performance in the real world.

Abstract

Robot manipulation in the real world is fundamentally constrained by the visual sim2real gap, where depth observations collected in simulation fail to reflect the complex noise patterns inherent to real sensors. In this work, inspired by the denoising capability of diffusion models, we invert the conventional perspective and propose a cleanto-noisy paradigm that learns to synthesize noisy depth, thereby bridging the visual sim2real gap through purely simulation-driven training. Building on this idea, we introduce RealD²iff, a hierarchical coarse-to-fine diffusion framework that decomposes depth noise into global structural distortions and fine-grained local perturbations. To enable progressive learning of these components, we further develop two complementary strategies: Frequency-Guided Supervision (FGS) for global structure modeling

and Discrepancy-Guided Optimization (DGO) for localized refinement. To integrate RealD² iff seamlessly into imitation learning, we construct a pipeline that spans six stages. We provide comprehensive empirical and experimental validation demonstrating the effectiveness of this paradigm. RealD² iff enables two key applications: (1) generating realworld-like depth to construct clean—noisy paired datasets without manual sensor data collection. (2) Achieving zeroshot sim2real robot manipulation, substantially improving real-world performance without additional fine-tuning.

1. Introduction

Policy learning [1, 3, 4] has achieved remarkable progress in robotic manipulation, enabling robots to acquire perception, planning, and control skills directly from demonstrations without handcrafted feature engineering. However, these approaches rely heavily on collecting large quantities of high-quality demonstrations. Real-world data acquisition typically follows two paradigms: human video demonstrations and teleoperation. Although human videos offer realistic visuals and dynamics, they lack temporally aligned robot actions and often operate in mismatched action spaces. Teleoperation alleviates this issue by providing aligned perception—action pairs, yet its high cost and limited scalability hinder its use for large-scale policy learning.

To reduce the burden of real-world data collection, simulation-based approaches [10, 24, 27] have become an attractive alternative. Simulators can efficiently generate diverse demonstrations at scale. Nevertheless, the "sim2real gap" remains a fundamental challenge, arising from discrepancies in both physics and visual appearance between simulation and the real world. Among these factors, the visual sim2real gap is particularly critical for manipulation tasks that depend heavily on spatial reasoning. For example, a robot must accurately perceive object geometry and pose to perform precise operations such as pouring water without spillage. With the widespread adoption of depth cameras, obtaining 3D information has become more accessible, but real depth sensors often introduce significant structured noise and artifacts. This depth gap severely impacts the fidelity of 3D perception in manipulation, yet has received surprisingly limited attention.

In this work, motivated by the denoising capability of diffusion models [13, 39, 50], we invert the conventional denoising perspective and propose a clean-to-noisy paradigm that learns to synthesize real-world-like depth directly from simulation. As illustrated in Fig. 1, this paradigm enables simulation to produce enhanced depth observations that exhibit real-world sensor characteristics. To assess the empirical feasibility of the clean-to-noisy paradigm, we conduct a distribution-level statistical analysis showing conditions under which diffusion-generated residuals approximate the statistical behavior of real sensor noise. Unlike conventional diffusion-based image translation removing noise in a noisy-to-clean fashion, our formulation targets the generation of highly uncertain noisy depth, making feasibility analysis particularly important for motivating our approach.

Building on this paradigm, we introduce **RealD**²**iff**, a hierarchical coarse-to-fine diffusion framework that decomposes depth noise into global structural distortions and finegrained local perturbations. To support this design, we propose Frequency-Guided Supervision (FGS) for capturing global deformations and Discrepancy-Guided Optimization (DGO) for refining local inconsistencies. In the coarse stage, we suppress high-frequency disturbances to focus on structural deviations, avoiding early overfitting to stochastic sensor artifacts. In the fine stage, we utilize discrepancy

regions from the preceding output to guide refinement, enhancing detailed noise generation in inconsistent areas.

To seamlessly integrate RealD²iff into imitation learning, we construct a comprehensive pipeline spanning simulation construction and alignment, demonstration collection and enhancement, and policy learning and deployment. To validate its **experimental feasibility**, we showcase two key applications: (1) generating realistic depth to construct clean—noisy paired datasets without any real-world sensor capture, and (2) enabling zero-shot sim2real transfer for manipulation tasks, significantly improving real-world policy performance without additional fine-tuning.

The contributions of this paper are threefold:

- We propose a clean-to-noisy paradigm to learn real-world-like noisy depth purely from clean simulation, providing a data-driven solution to the visual sim2real gap. We further explore statistical justification that outlines the empirical feasibility and conditions of this paradigm.
- We introduce RealD²iff, a hierarchical coarse-to-fine diffusion framework that decomposes depth noise into global and local components. With FGS and DGO strategies, RealD²iff enhances simulated depth offline, enabling policy learning under perception conditions that are equivalent to physical world.
- We construct a complete end-to-end robotic learning pipeline with RealD²iff covering six key stages, and demonstrate two key applications in real-world-like depth generation and zero-shot sim2real robot manipulation across 4 policies and 4 tasks.

2. Related Work

2.1. Learning Manipulation from Demonstrations

Imitation learning[3, 4, 37] is a key approach for training robot policies from demonstration data[28, 43], where policies learn to predict actions based on state-action pairs. This technique has been widely applied in robot manipulation, with recent work extending to both single-task[3, 57] and multi-task policies[1, 20, 23, 47] using RGB images from various camera setups[2, 8]. However, these methods struggle to generalize across different visual conditions. To address this limitation, recent approaches[15, 52, 54] have started incorporating 3D representations, such as point clouds or depth data, to improve policy generalization. However, they still face challenges in dealing with noise from depth sensors and require significant preprocessing, such as point cloud downsampling and calibration. Additionally, some works focus on training policies with depthonly data[26] or 3D-aware models[58] to enhance visual perception. While promising, due to the cost of collecting large amount of high-quality demonstrations, these methods are often confined to simulated environments, making it difficult to achieve zero-shot transfer to real-world settings.

2.2. Visual Sim2Real Transfer for Robotics

Sim2Real transfer involves overcoming both the physics gap and perception gap between simulated and real-world environments. The physics gap, including discrepancies in dynamics and friction, is commonly addressed by domain randomization[32, 42] or domain adaptation[7, 40], where policies are trained to handle a range of simulated physical conditions. While this approach is effective for locomotion tasks[41], manipulation tasks[31] require more precise visual modeling since they depend heavily on accurate object observations, typically provided by RGB or depth images. For manipulation, high-fidelity simulation rendering is essential to reduce the visual gap, but even with advancements in rendering technologies [49], relying on simulation alone often requires extensive augmentations and curriculum design[45] for successful transfer. Some approaches[12, 22, 59, 60] have moved beyond RGB, using depth and point cloud data to mitigate visual discrepancies, yet these still require noise augmentation in simulation or significant post-processing in camera to handle visual gap. However, existing methods that add noise to simulation data[15, 26, 50] struggle to capture the full complexity of real-world patterns and are confined to simulation environments, leading to a loss of geometric accuracy in robot manipulation. In contrast, methods that focus on denoising real-world data[25, 27] often place policies in an idealized training environment, reducing robustness to uncertain noises and limiting generalization to unseen scenarios.

2.3. Diffusion-based Generative Model

We approach the visual Sim2Real transfer problem by learning the mapping between synthetic noise and noise captured in the real world, focusing on depth images. In the field of generation and translation, a range of generative models have been explored, such as Generative Adversarial Networks (GANs)[9] and Variational Autoencoders (VAEs)[21]. Among these, diffusion models have gained significant attention due to their more stable training processes and ability to generate high-quality images with superior preservation of fine details [14, 34]. Recently, depth diffusion models have emerged as a promising tool. These models primarily focus on depth estimation tasks in both monocular [5, 18, 36] and multi-view settings [19, 46, 50]. Other studies have extended diffusion-based approaches to traditional image translation tasks, such as depth map superresolution[38] and depth refinement [56], which aim to generate clean and deterministic output. In contrast, our work adopts a generative approach with the goal of 'generating noise'. The uncertain desired output makes the underlying distribution more complex and introducing fundamentally different challenges. This distinction sets our work apart, focusing on modeling and generating noise patterns to better handle the uncertainty inherent in real-world depth.

3. Method

3.1. RealD2iff: Hierarchical Diffusion Framework

Problem Formulation. Given an collected observation $\mathcal{O}^t = \{r_i^t, g_i^t, b_i^t, d_i^t, \mathcal{S}_i^t\}$ at time t, where $(r_i^t, g_i^t, b_i^t, d_i^t)$ denote the RGB-D measurements of the scene, \mathcal{S}_i^t represents the joint states of robot. \mathcal{A}^t is the corresponding executed actions. The imitation objective is to learn a manipulation policy $\pi_\theta: \mathcal{O}^t \to \hat{\mathcal{A}}^t = \{\hat{A}_{t+1}, \hat{A}_{t+2}, \dots, \hat{A}_{t+n}\}$ that predicts the next-step actions from perception and proprioception. However, due to the substantial discrepancy in depth sensing, i.e., between simulated depth \mathcal{D}^{sim} and real-world depth $\mathcal{D}^{\text{real}}$, directly learning a mapping $\mathcal{F}: \mathcal{D}^{\text{sim}} \to \mathcal{D}^{\text{real}}$ is intractable. To tackle it, RealD²iff decomposes it into two sub-mappings $\mathcal{H}_1: \mathcal{D}^{\text{sim}} \to \hat{\mathcal{D}}^{\text{coarse}}$ and $\mathcal{H}_2: \mathcal{D}^{\text{sim}} \to \hat{\mathcal{D}}^{\text{fine}}$ realized by hierarchical diffusion model that progressively learn from coarse global structure to fine local details.

Overview. RealD²iff introduces a hierarchical coarse-tofine diffusion framework to synthesize realistic depth noise in a structured manner, shown in Fig.2. The coarse diffusion model \mathbb{D}_c first estimates a global structural noise field Δ_c and a discrepancy map \mathcal{M} from clean simulated depth \mathcal{D}^{sim} , capturing large-scale geometric deviations and highlighting high-discrepancy regions between simulated and real distributions. The resulting coarse depth $\hat{\mathcal{D}}^{\text{coarse}} =$ $\mathcal{D}^{\mathrm{sim}} + \Delta_c$ encodes the global deformation structure. Conditioned on $(\hat{\mathcal{D}}^{\text{coarse}}, \mathcal{M})$, the fine diffusion model \mathbb{D}_f further refines local perturbation noise Δ_f with discrepancyguided adaptive weighting, generating the final real-worldlike depth $\hat{\mathcal{D}}^{\text{fine}} = \hat{\mathcal{D}}^{\text{coarse}} + \Delta_f$. The hierarchical decomposition showing converge more easily and yield better performance compared to E2E paradigm, enables RealD²iff to learn both global consistency and local perturbation. This provides a principled mechanism to construct noise-aware real-world observation for visuomotor policy learning, ensuring zero-shot sim2real transfer without requiring additional real-world data for fine-tuning.

3.2. Coarse Stage: Global Structural Initialization

Preliminaries on Diffusion Models. RealD²iff builds upon [13, 39], which approximate a data distribution $p(\mathcal{D})$ by learning a parameterized reverse process to gradually denoise a sample from Gaussian noise. The diffusion process consists of two Markov chains: a *forward process* that corrupts clean data by adding Gaussian noise, and a *reverse process* that learns to reconstruct data from the noisy version. Specifically, given a clean depth map \mathcal{D}_0 , the forward process produces a noisy version $\mathcal{D}_t = \sqrt{\alpha_t}\mathcal{D}_0 + \sqrt{1-\alpha_t}\epsilon$, where $\epsilon \sim \mathcal{N}(\mathbf{0}, \mathbf{I})$ and α_t controls the noise schedule. The reverse process learns a denoising network $\mu_{\theta}^{\epsilon}(\mathcal{D}_t, t)$ to iteratively predict and remove ϵ from \mathcal{D}_t , with the objective \mathcal{L}_{θ} . For further details on the prior, please refer to APPENDIX.

$$\mathcal{L}_{\theta} = \mathbb{E}_{\boldsymbol{\epsilon},t} \| \boldsymbol{\epsilon} - \boldsymbol{\mu}_{\theta}^{\boldsymbol{\epsilon}}(\mathcal{D}_{t},t) \|^{2}$$
 (1)

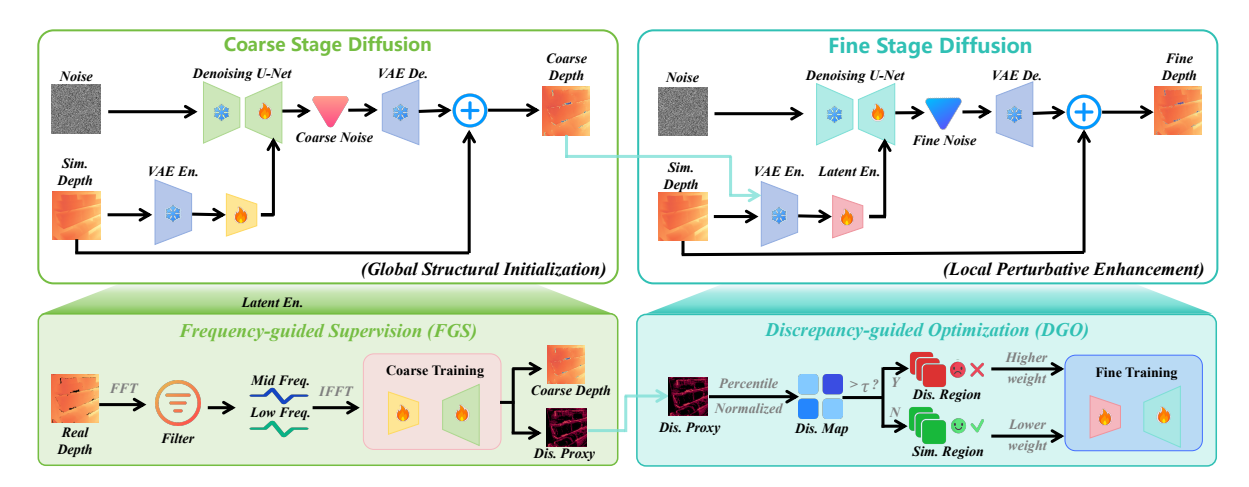


Figure 2. The overview of RealD²iff's framework. Coarse Stage Diffusion(Sec. 3.2), guided by FGS, filters high-frequency patterns to characterize global deformation, allowing stable geometric correspondence. Fine Stage Diffusion(Sec. 3.3), guided by DGO, focuses on discrepancy and optimizes fine-grained perturbation details. Progressive framework enhances depth realism through coarse-to-fine training.

Global Structural Noise Generation. Stage-I aims to synthesize global structural noise Δ_c , corresponding to mid- and low-frequency components that describe depth bias, scale drift, and surface deformation. To ensure the diffusion model \mathbb{D}_c focuses on these global structures rather than high-frequency perturbations, we introduce a frequency-guided supervision strategy. Given the ground-truth noise $\Delta_c^* = \mathcal{D}^{\rm real} - \mathcal{D}^{\rm sim}$, we apply high-pass filter $\mathcal{F}_{\rm HP}$ in the Fourier domain to obtain its structural component $\bar{\Delta}_c^* = \Delta_c^* - \mathcal{F}_{\rm HP}(\Delta_c^*)$. Conditioned on $\mathcal{D}^{\rm sim}$, \mathbb{D}_c learns to approximate the distribution $p(\bar{\Delta}_c|\mathcal{D}^{\rm sim})$ via denoising supervised by $\bar{\Delta}_c^*$. The objective function is formulated as:

$$\mathcal{L}_{\text{struct}} = \mathbb{E}_{\boldsymbol{\epsilon},t} \| \boldsymbol{\epsilon} - \boldsymbol{\mu}_{\theta}^{\boldsymbol{\epsilon}}(\bar{\Delta}_{c,t}, t, \ell_{\theta}(\mathcal{D}_{t}^{\text{sim}})) \|^{2}, \quad (2)$$

where $\bar{\Delta}_{c,t}$ denotes the noisy version of $\bar{\Delta}_c^*$ at time step t and ℓ_{θ} denotes the latent encoder. This frequency-aware loss effectively constrains the model to capture structural deformations while avoiding over-fitting to stochastic sensor noise, leading to the coarse prediction $\hat{\mathcal{D}}^{\mathrm{coarse}} = \mathcal{D}^{\mathrm{sim}} +$ Δ_c that reflects global geometry alignment with real depth. Discrepancy Map for Region Identification. Although $\hat{\mathcal{D}}^{\text{coarse}}$ captures global structural deformation, residual inconsistencies still appear in fine-grained regions. To localize these areas, the coarse model is extended to jointly predict a discrepancy proxy \mathcal{M}_0 alongside Δ_c , where \mathcal{M}_0 estimates the pixel-wise deviation between the coarse prediction and the real depth distribution. We further aggregate $\hat{\mathcal{M}}_0$ over non-overlapping 8×8 blocks to obtain a regionlevel discrepancy map $\mathcal{M} = \text{Pool}_{8\times8}(\hat{\mathcal{M}}_0)$. Each block value thus reflects the model's confidence regarding structural reliability within that region, providing a compact and interpretable spatial uncertainty signal. The map is normalized to [0, 1] and passed as auxiliary guidance, enabling the overall mapping $\mathcal{F}: \mathcal{D}^{\mathrm{sim}} \to \mathcal{D}^{\mathrm{real}}$ to consistently integrate global bias and localized perturbation during refinement.

3.3. Fine Stage: Local Perturbative Enhancement

Discrepancy-Guided Optimization. In the local perturbative enhancement, the discrepancy map \mathcal{M} derived in Stage-I serves as a region-wise importance prior that adaptively modulates the optimization focus. Regions exhibiting high discrepancy values correspond to unsatisfactory areas where the coarse model diverges from the real depth distribution, while low-discrepancy regions indicate relatively satisfactory predictions. To explicitly leverage this spatial prior, we partition the entire depth domain into two disjoint subsets: $\Omega_{\rm dis} = \{p \,|\, \mathcal{M}(p) > \tau\}$ and $\Omega_{\rm sim} = \{p \,|\, \mathcal{M}(p) \leq \tau\}$, where τ is a fixed threshold (empirically $\tau = 0.3$). The fine diffusion model \mathbb{D}_f thus focuses its refinement on $\Omega_{\rm dis}$, while softly preserving structures within $\Omega_{\rm sim}$.

Local Perturbation Noise Enhancement. Conditioned on both the coarse output $\hat{\mathcal{D}}^{\text{coarse}}$ and the discrepancy map \mathcal{M} , the fine diffusion model \mathbb{D}_f learns to model the conditional distribution $p(\Delta_f|\hat{\mathcal{D}}^{\text{coarse}},\mathcal{M})$, capturing residual high-frequency perturbations such as stochastic jitter, edge misalignment, or reflection artifacts. Following the standard denoising objective Eq.1, the training loss is defined as:

$$\mathcal{L}_{\phi} = \mathbb{E}_{\epsilon, t} \| \epsilon - \boldsymbol{\mu}_{\phi}^{\epsilon}(\Delta_{f, t}, t, \ell_{\phi}(\hat{\mathcal{D}}^{\text{coarse}}, \mathcal{M})) \|^{2}.$$
 (3)

To emphasize refinement in unsatisfactory regions, we reweight this objective according to the discrepancy partition:

$$\mathcal{L}_{\text{fine}} = \omega \, \mathbb{E}_{p \in \Omega_{\text{sim}}} [\mathcal{L}_{\phi}(p)] + \lambda \, \mathbb{E}_{p \in \Omega_{\text{dis}}} [\mathcal{L}_{\phi}(p)] \,, \tag{4}$$

where ω and λ are weighting coefficients, setting $\omega=0.5$ and $\lambda=1.5$ yields better trade-off between preservation and enhancement. This discrepancy-weighted loss effectively guides \mathbb{D}_f to allocate greater gradient capacity to uncertain regions. The final refined prediction is then obtained as $\hat{\mathcal{D}}^{\text{fine}}=\hat{\mathcal{D}}^{\text{coarse}}+\Delta_f$, completing the hierarchical refinement process, achieving localized perturbation correction.

3.4. Why Diffusion Promotes Real-world-like?

This section offers an empirical and distribution-level perspective on why diffusion-generated residuals can exhibit real-world-like characteristics when added to simulator depth. The goal is not to establish strict equivalence but to discuss under what practical and observable conditions diffusion serves as a suitable mechanism for modeling depth.

For each simulated depth $\mathcal{D}^{\mathrm{sim}}$, we model the corresponding real observation as $\mathcal{D}^{\mathrm{real}} = \mathcal{D}^{\mathrm{sim}} + \delta$, where δ represents real-world noise. A diffusion-based generative model is trained to approximate this residual distribution. The predicted depth map is given by $\hat{\mathcal{D}}^{\mathrm{fine}} = \mathcal{D}^{\mathrm{sim}} + \Delta$. Here, Δ captures the discrepancy between the simulated and real-world depth. The goal is to determine when this predicted noise Δ results in a synthesized depth distribution $\hat{\mathcal{D}}^{\mathrm{fine}}$ that matches the real-world depth distribution $\mathcal{D}^{\mathrm{real}}$.

Assumptions and Statistical Setting. To establish statistical equivalence, we introduce empirically verifiable assumptions. A1 can be empirically checked via residual statistics, A2 can be reflected in diffusion validation, and A3 naturally holds in bounded robotic manipulation scenes.

- **A1.** Conditional Moment Stability: For each $\mathcal{D}^{\mathrm{sim}}$, the real residual distribution admits stable first and second moments, i.e., there exist measurable functions that: $\mathbb{E}[\delta] = \mu(\mathcal{D}^{\mathrm{sim}})$ and $\mathrm{Cov}[\delta] = \Sigma(\mathcal{D}^{\mathrm{sim}})$.
- **A2.** Generative Approximation: The Diffusion model approximates the conditional residual distribution within bounded divergence: $\mathrm{KL}(p_{\delta}\|p_{\Delta}) \leq \varepsilon_{\mathrm{KL}}(\mathcal{D}^{\mathrm{sim}})$, equivalently in TV distance[6]: $\mathrm{TV}(p_{\delta},p_{\Delta}) \leq \varepsilon_{\mathrm{TV}}(\mathcal{D}^{\mathrm{sim}})$.

A3. Bounded Support: The marginal distribution of simulated depth $p_{\mathcal{D}^{\mathrm{sim}}}$ has bounded support or rapidly decaying tails, ensuring integrability and stable convolution behavior. **Empirical Distribution-Level Insight.** The marginal distributions of real and generated depth maps are conditional mixtures over the simulator distribution. The TV distance between these two distributions is bounded by:

$$\operatorname{TV}(p_{\mathcal{D}^{\text{real}}}, p_{\hat{\mathcal{D}}^{\text{fine}}}) \leq \mathbb{E}\left[\operatorname{TV}(p_{\delta}, p_{\Delta})\right].$$
 (5)

This indicates that the discrepancy between real and generated depth distributions is determined by the expected TV distance between the real and predicted residuals. By Pinsker's inequality, we apply the KL divergence to TV:

$$TV(p_{\delta}, p_{\Delta}) \le \sqrt{\frac{1}{2}KL(p_{\delta}||p_{\Delta})}.$$
 (6)

Substitute Eq.5,6 into the approximation bound in A2 gives:

$$\text{TV}(p_{\mathcal{D}^{\text{real}}}, p_{\hat{\mathcal{D}}^{\text{fine}}}) \le \mathbb{E}\left[\sqrt{\frac{1}{2}\varepsilon_{\text{KL}}(\mathcal{D}^{\text{sim}})}\right].$$
 (7)

If there exists a uniform upper bound $\varepsilon_{\mathrm{KL}}(\mathcal{D}^{\mathrm{sim}}) \leq \varepsilon$:

$$\operatorname{TV}(p_{\mathcal{D}^{\operatorname{real}}}, p_{\hat{\mathcal{D}}^{\operatorname{fine}}}) \le \sqrt{\frac{\varepsilon}{2}}.$$
 (8)

During diffusion training, the KL term is iteratively minimized via denoising score matching; thus, the upper bound $\varepsilon \to 0$ as training converges, leading to asymptotic equivalence between predicted and real depth distributions. In the case where the residuals δ and Δ follow Gaussian distributions, the closed-form expression of the KL divergence (refer to APPENDIX) further clarifies how the residual distribution properties affect the divergence bound.

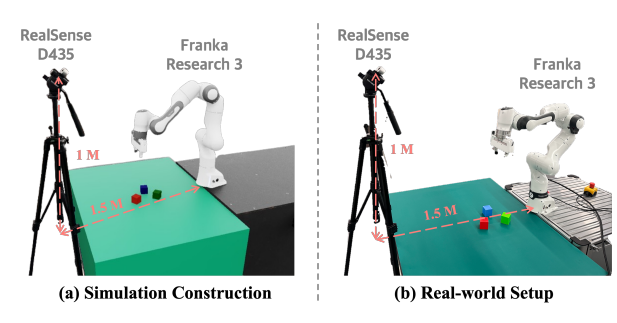


Figure 3. Manipulation construction with Franka Research 3 and RealSense D435. (a) The training environments for manipulation tasks in the simulation. (b) The real-world deployment environment. The geometric shapes and spatial information are strictly aligned, while the color and background environment are kept similar but not necessarily identical. This ensures that the task-relevant visual cues are consistent, while allowing flexibility.

4. Manipulation with RealD²iff

RealD²iff enables the generation of real-world-like depth images within simulation, allowing simulation to be effectively used for learning manipulation policies, which can then be seamlessly transferred to real-world robots. To evaluate the efficacy of RealD²iff in robotic manipulation, we propose a depth-aware sim²real pipeline that covers six stages. The trained policy is deployed on real robots, with RealD²iff used as an offline plug-in to enhance depth data.

4.1. Simulation Construction & Alignment

We leverage RGB-D data in an object-centric robotic manipulation setting. This allows us to focus on geometric similarity between objects in the simulation and the real world, without requiring exact alignment of backgrounds or object appearances during simulation construction, as shown in Fig.3. Once the simulation environment is constructed, we set up the camera to capture RGB-D visual observations. For camera alignment, we use a differentiablerendering-based camera calibration method, which estimates the camera extrinsics with minimal human input. However, perfect alignment is difficult due to differences in the camera models between the simulation and real-world sensors. To account for these discrepancies, we introduce slight randomization of camera poses. This helps the policy become more robust to small misalignments and ensures better performance when deployed in the real world.

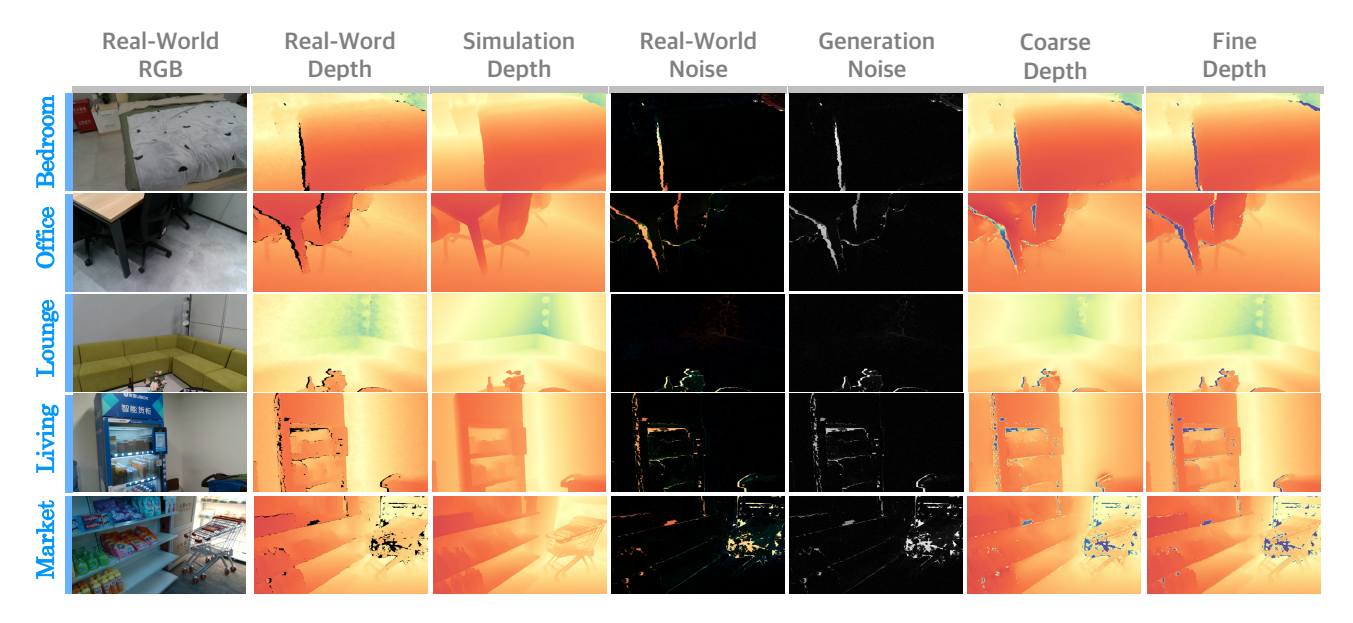


Figure 4. The visualization of the depth enhanced by RealD2iff across diverse scenes. Refer to the APPENDIX for more scenes.

4.2. Demonstration Generation & Enhancement

To efficiently obtain expert demonstrations within simulation, we build upon the MimicGen framework [29] and incorporate a whole-body control scheme [11] to produce smoother and more consistent trajectories. Our data collection pipeline further integrates several practical enhancements, such as randomized resets for retry generation, adaptive velocity modulation for precise motion refinement, and other utilities that improve demonstration quality and diversity. Additional implementation details and algorithmic descriptions are provided in the APPENDIX.

4.3. Policy Learning & Deployment

While several recent policies leverage point-cloud inputs for improved robustness [15, 44, 53], these methods still rely on depth-camera measurements converted into point clouds, requiring aggressive handcraft to suppress artifacts. In contrast, we follow a similar high-level policy design but operate directly on RGB-D observations. To accommodate depth more effectively, we modify the visual backbone by extending the pretrained ResNet to include an additional depth stream, and a dedicated depth branch is fused with other visual-proprioceptive embeddings before processed by the diffusion head to predict the action sequence. The full observation space includes RGB-D images, robot joint positions, and gripper status. During real-world deployment, RealD²iff is applied offline to simulate depth realism. The enhanced depth maps produced by RealD2iff serve as the visual input for policy learning, enabling the trained policy to transfer to physical robots without requiring online correction or depth-domain adaptation at inference time.

5. Experiment

The experiments are designed to evaluate the threefold:

- Can RealD²iff generate real-world-like noisy depth maps from clean simulation depth?
- Does depth enhancement using RealD²iff effectively bridge the visual sim2real gap in robot manipulation?
- How do the noise modeling design, the generative framework, and the training strategy contribute to the effectiveness of RealD²iff?

5.1. Performance of Depth Generation

Experimental Setup. It is important to clarify that we use generic depth captured to construct clean-noisy depth pairs from public datasets[25, 27] for diffusion training without real-world robots or expert trajectories. It's not conflict with the simulation-driven robotic policy learning. We train our RealD²iff using two 24GB Nvidia GeForce RTX 4090 GPUs, fine-tuning the official SD-V2.1 model[35]. ByteCameraDepth[27] contains real-world raw depth data collected from 7 cameras across 10 modes in 7 different scenes and provides camera denoising models, which can be used to construct scene-level pairs. LASA[25] contains 10,412 CAD models across 17 object categories, providing object-level pairs rendered on camera information.

Compared Methods. Since our method operates on depth images, we select several image-to-image translation methods for comparison: 1) Pix2Pix[16], a classical image generation method. 2) Giga-GAN[17], a state-of-the art GAN-based method. 3) Stable Diffusion[35], our main baseline model. 4) ControlNet [55], an extension of SD that allows precise control by conditioning on additional inputs. We adapt these methods to predict 1-channel 16-bit depth.

Dataset	Method	Bedroom	Office	Living	Lounge	Market
Out-of-domain	Pix2Pix [16]	37.2 / 10.1 / 13.7	35.6 / 11.2 / 12.5	52.4 / 9.38 / 21.7	54.8 / 9.04 / 24.3	45.6 / 8.98 / 17.3
	Giga-GAN [17]	40.1 / 8.26 / 15.1	41.4 / 7.74 / 16.3	54.3 / 8.12 / 22.1	59.4 / 7.13 / 26.0	47.3 / 9.01 / 16.8
	Stable-Diffusion [35]	40.2 / 8.21 / 16.2	41.9 / 7.47 / 16.6	51.1 / 7.14 / 21.9	60.3 / 7.08 / 26.8	52.2 / 7.05 / 21.8
	ControlNet [55]	48.4 / 7.31 / 19.5	50.4 / 6.93 / 22.3	59.7 / 5.82 / 24.7	62.6 / 5.35 / 28.8	54.1 / 5.61 / 22.3
	RealD2iff (ours)	51.8 / 4.63 / 22.1	53.5 / 4.49 / 25.7	60.6 / 5.57 / 26.4	63.1 / 5.36 / 28.5	55.3 / 5.23 / 23.8
	Pix2Pix [16]	45.3 / 7.15 / 17.9	45.2 / 7.98 / 18.5	53.8 / 9.01 / 19.8	56.5 / 8.24 / 25.1	50.6 / 7.58 / 16.9
In-domain	Giga-GAN [17]	52.9 / 6.01 / 21.1	53.4 / 5.74 / 23.3	54.6 / 8.05 / 22.6	57.4 / 7.83 / 25.5	52.3 / 7.21 / 19.4
	Stable-Diffusion [35]	51.6 / 6.11 / 20.3	52.9 / 6.47 / 21.6	52.3 / 6.48 / 22.3	58.5 / 7.01 / 26.9	54.2 / 6.25 / 22.3
	ControlNet [55]	60.3 / 4.91 / 25.5	58.4 / 4.23 / 25.2	61.7 / 4.86 / 27.7	61.6 / 6.92 / 27.5	57.1 / 5.33 / 25.6
	RealD2iff (ours)	62.6 / 4.13 / 27.8	62.9 / 4.09 / 28.1	66.5 / 2.45 / 31.8	66.2 / 3.58 / 30.6	60.3 / 4.21 / 27.2

Table 1. Comparison of translation performance on both scene-level and object-level depth construction across two experimental settings. In-domain refers to training the model on both datasets, excluding the validation set. Zero-shot OoD refers to training the model on LASA and validating it on ByteCameraDepth, and vice versa. Evaluation metrics are mIoU / Chamfer L2 / F-score respectively, where the focus is on assessing the fidelity of noisy depth relative to the real-world GT on both object-level and scene-level. Further details are shown in the Appendix. Higher mIoU and F-score are better while lower Chamfer L2 is better. Chamfer L2 is scaled by 1,000 times.

Visualization results. We present the visualization results of depth maps generated by RealD²iff for five different scenes: bedroom, office, living room, lounge, and market, as shown in Fig.4. These results clearly demonstrate the accuracy and generalization capability of RealD²iff in generating real-world-like noisy depth. Additional visualizations for more scenes and objects can be found in APPENDIX.

Quantitative results. We evaluate the quality of depth construction on both scene-level and object-level through two sets of comparative experiments, designed with cross-validation for zero-shot Out-of-domain and In-domain settings. Tab.1 compares the noisy depth generated by different methods. The results demonstrate that the noisy depth data generated by our model closely resembles real-world collected data, and the hierarchical coarse-to-fine generation framework provides significant generalization ability in noisy depth generation of different domain.

5.2. Performance of Sim2Real Robot Manipulation

Experimental Setup. In the real-world setup, we employ the Franka Research 3 robot arm, equipped with a Franka 2-finger parallel gripper. Depth data is captured using the RealSense D435 camera, positioned at a fixed location with coordinates (1m, 1.5m) relative to the base coordinate system of the robot arm. In the simulation setup, the environment is constructed in Isaac Sim 5.0.0, where the digital assets are aligned to match the real-world setup.

Compared Policies. Note that our goal is not to compare whether noisy depth leads to better training performance than clean depth. Instead, we aim to validate whether the noise embedded in the generated depth images helps mitigate the sim2real gap. we modify the visual backbone of the selected policies by adding depth channel (see Sec. 4.3). The robot learning policies we selected for comparison are: 1) Diffusion Policy [3]: A representative robot's visuomotor policy. 2) PPT [15]: A multi-task policy architecture, called proprioceptive point-cloud transformer. 3) CAGE [48]: A

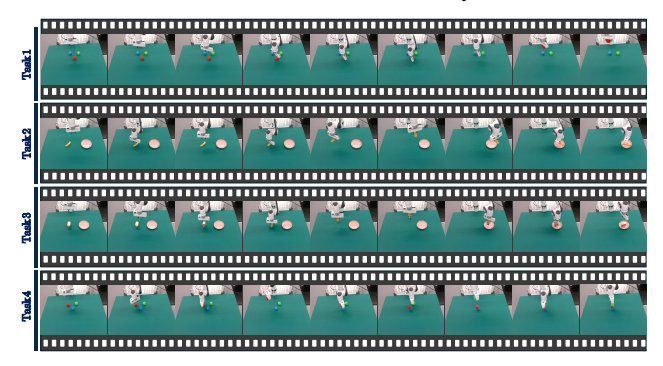


Figure 5. **Visualization of real-world operation demos.** The four tasks range from precise grasping, flexible controlling to triple stacking, corresponding to four operations of increasing difficulty.

policy leveraging a causal attention mechanism for robust generalization across diverse environment. 4) RISE [44]: A robot manipulation policy that predicts continuous actions directly from single-view point clouds.

Visualization results. We designed four manipulation tasks in increasing order of difficulty, as follows: 1) Pick Cube. 2) Place Banana. 3) Can-to-Plate. 4) Stack Cube. For each task, we collected 900 demonstration trajectories in the simulation, trained the policies using imitation learning, and then deployed them with the integration of RealD²iff. The tasks setup, shown in Fig.5, involved testing at 10 different locations with 3 trials at each location.

Quantitative results. Tab.2 summarizes the zero-shot sim2real transfer validation results, comparing the performance of four policies across three settings: (a) simulation performance using clean depth, (b) real-world performance using clean depth, and (c) real-world performance using depth enhanced by RealD2iff. We observed the following key findings: (1) All policies demonstrated excellent performance in the simulation environment with clean depth data. However, when evaluated in a noisy depth real-world environment, their performance deteriorated to varying de-

Method	Diffusion Policy[3]		PPT[15]		CAGE[48]		RISE[44]					
Method	sim	real(w/o)	real(w.)	sim	real(w/o)	real(w.)	sim	real(w/o)	real(w.)	sim	real(w/o)	real(w.)
Pick Cube	30/30	8/30	30/30	30/30	16/30	30/30	30/30	12/30	30/30	30/30	15/30	30/30
Place Banana	27/30	7/30	25/30	29/30	11/30	30/30	28/30	9/30	27/30	28/30	12/30	30/30
Can-to-Plate	22/30	1/30	19/30	24/30	15/30	24/30	23/30	7/30	23/30	22/30	4/30	21/30
Stack Cube	21/30	2/30	20/30	25/30	10/30	23/30	24/30	7/30	21/30	23/30	8/30	24/30

Table 2. **Zero-shot sim2real results using RealD2iff in the real-world robot pipeline.** The experiment provides three validation settings for each policy. In this table, sim represents setting(a), real(w/o) represents setting(b) and real(w) represents setting(c).

Augmentation	FID↓	Chamfer L2↓	Real SR↑
Baseline (Sim only)	401.3	28.26	0.25
+ Gaussian depth noise	227.1	23.47	0.52
+ Perlin depth noise	235.6	23.21	0.58
+ ActiveDR [30]	191.2	14.36	0.65
+ UniDepth [33]	134.6	5.12	0.78
+ DepthAnything [51]	100.4	4.75	0.81
+ RealD ² iff (ours)	76.7	3.62	0.92

Table 3. Comparison of different augmentation baselines. Evaluated on depth realism (FID, Chamfer L2) and real-world Stack-Cube task (SR). RealD²iff achieves the best depth fidelity and the highest manipulation performance.

grees, with PPT[15] showing the least degradation. (2) After training on the depth enhanced by RealD²iff, four policies showed improved performance in the real-world environment compared to their performance without enhancement, with performance remaining close to the simulation level. This demonstrates that RealD²iff effectively bridges the depth gap and enables zero-shot sim²real transfer.

5.3. Effectiveness Studies of RealD²iff

Impact of Noise Modeling Choices. To examine how different depth—noise generation paradigms affect both depth realism and downstream sim2real manipulation, we compare RealD²iff against a set of representative baselines, including analytic sensor-noise models: Gaussian and Perlin noise, advanced domain randomization technique: ActiveDR [30], and SOTA monocular depth estimation models: UniDepth [33], DepthAnything [51]. We evaluate two types of performance, as shown in Tab. 3: (1) Depth realism, using FID to measure distributional similarity and Chamfer L2 to quantify geometric deviation between generated and real depth. (2) Downstream robot manipulation, using Success Rate (SR) on the Stack-Cube task conducted in the real world. Further details are shown in the Appendix.

Impact of Generative Frameworks. One of the key advantages of RealD²iff is its coarse-to-fine framework, compared to traditional E2E approaches. It provides two benefits: (1) Allowing model to accumulate representational priors from a simpler coarse-level task, thereby easing the optimization of subsequent fine-level learning and mitigating premature convergence to sub-optimal minima. (2) En-

Metrics	E2E	w/o FGS	w/o DGO	FGS + DGO
mIoU↑	53.9	60.4	58.3	63.7
Chamfer L2 ↓	6.64	4.11	4.39	3.70
F-score↑	22.8	26.7	25.8	29.1

Table 4. Ablation studies on different strategies of RealD2iff.

abling each level to employ specialized loss objectives and tailored optimization schedules, allowing more effective supervision at different spatial scales. We conduct ablation experiments to compare different frameworks in Fig.6.(a). **Impact of Training Strategies.** Based on an effective generative framework design, we also propose FGS and DGO strategies in progressive training to more effectively improve generative performance. We visualized the Discrepancy Maps of the DGO strategy in Fig.6.(b). To evaluate the impact of each key design, we conduct quantitative ablations of in-domain generation tasks on different strategies of RealD²iff. The result is summarized in Tab. 4.

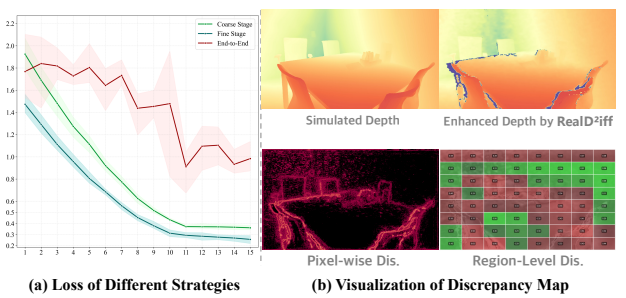


Figure 6. Ablation studies of frameworks & strategies

6. Conclusion

In this paper, we present RealD2iff, a hierarchical coarse-to-fine depth diffusion to address the long-standing visual depth sim2real gap in robot manipulation. We propose a novel clean-to-noisy paradigm that generates real-world-like depth enabling significantly robust policy learning within simulation demonstration. Our integrated pipeline collectively offers a general and effective recipe, providing not only a practical solution but also a new perspective for advancing embodied intelligence under real-world constraints. We will further explore the transfer effectiveness in more complex environments and operations such as transparent, reflective and articulated objects' manipulation.

References

- [1] Kevin Black, Noah Brown, Danny Driess, Adnan Esmail, Michael Equi, Chelsea Finn, Niccolo Fusai, Lachy Groom, Karol Hausman, Brian Ichter, et al. π₀: A vision-languageaction flow model for general robot control. arXiv preprint arXiv:2410.24164, 2024. 1, 2
- [2] Cheng Chi, Zhenjia Xu, Chuer Pan, Eric Cousineau, Benjamin Burchfiel, Siyuan Feng, Russ Tedrake, and Shuran Song. Universal manipulation interface: In-the-wild robot teaching without in-the-wild robots. *arXiv preprint arXiv:2402.10329*, 2024. 2
- [3] Cheng Chi, Zhenjia Xu, Siyuan Feng, Eric Cousineau, Yilun Du, Benjamin Burchfiel, Russ Tedrake, and Shuran Song. Diffusion policy: Visuomotor policy learning via action diffusion. *The International Journal of Robotics Research*, 44 (10-11):1684–1704, 2025. 1, 2, 7, 8
- [4] Michael Drolet, Simon Stepputtis, Siva Kailas, Ajinkya Jain, Jan Peters, Stefan Schaal, and Heni Ben Amor. A comparison of imitation learning algorithms for bimanual manipulation. *IEEE Robotics and Automation Letters*, 2024. 1, 2
- [5] Yiquan Duan, Xianda Guo, and Zheng Zhu. Diffusiondepth: Diffusion denoising approach for monocular depth estimation. In *European Conference on Computer Vision*, pages 432–449. Springer, 2024. 3
- [6] Alexei A Fedotov, Peter Harremoës, and Flemming Topsoe. Refinements of pinsker's inequality. *IEEE Transactions on Information Theory*, 49(6):1491–1498, 2003. 5
- [7] Nolan Fey, Gabriel B Margolis, Martin Peticco, and Pulkit Agrawal. Bridging the sim-to-real gap for athletic locomanipulation. arXiv preprint arXiv:2502.10894, 2025. 3
- [8] Zipeng Fu, Tony Z Zhao, and Chelsea Finn. Mobile aloha: Learning bimanual mobile manipulation with low-cost whole-body teleoperation. arXiv preprint arXiv:2401.02117, 2024. 2
- [9] Ian Goodfellow, Jean Pouget-Abadie, Mehdi Mirza, Bing Xu, David Warde-Farley, Sherjil Ozair, Aaron Courville, and Yoshua Bengio. Generative adversarial networks. *Communications of the ACM*, 63(11):139–144, 2020. 3
- [10] Xiaoshen Han, Minghuan Liu, Yilun Chen, Junqiu Yu, Xiaoyang Lyu, Yang Tian, Bolun Wang, Weinan Zhang, and Jiangmiao Pang. Re³sim: Generating high-fidelity simulation data via 3d-photorealistic real-to-sim for robotic manipulation. arXiv preprint arXiv:2502.08645, 2025. 2
- [11] Jesse Haviland, Niko Sünderhauf, and Peter Corke. A holistic approach to reactive mobile manipulation. *IEEE Robotics and Automation Letters*, 7(2):3122–3129, 2022. 6
- [12] Tairan He, Chong Zhang, Wenli Xiao, Guanqi He, Changliu Liu, and Guanya Shi. Agile but safe: Learning collision-free high-speed legged locomotion. *arXiv preprint arXiv:2401.17583*, 2024. 3
- [13] Jonathan Ho, Ajay Jain, and Pieter Abbeel. Denoising diffusion probabilistic models. In *Proceedings of the 34th International Conference on Neural Information Processing Systems*, pages 6840–6851, 2020. 2, 3
- [14] Jonathan Ho, Chitwan Saharia, William Chan, David J Fleet, Mohammad Norouzi, and Tim Salimans. Cascaded diffu-

- sion models for high fidelity image generation. *Journal of Machine Learning Research*, 23(47):1–33, 2022. 3
- [15] Pu Hua, Minghuan Liu, Annabella Macaluso, Yunfeng Lin, Weinan Zhang, Huazhe Xu, and Lirui Wang. Gensim2: Scaling robot data generation with multi-modal and reasoning llms. arXiv preprint arXiv:2410.03645, 2024. 2, 3, 6, 7, 8
- [16] Phillip Isola, Jun-Yan Zhu, Tinghui Zhou, and Alexei A Efros. Image-to-image translation with conditional adversarial networks. In CVPR, 2017. 6, 7
- [17] Minguk Kang, Jun-Yan Zhu, Richard Zhang, Jaesik Park, Eli Shechtman, Sylvain Paris, and Taesung Park. Scaling up gans for text-to-image synthesis. In CVPR, 2023. 6, 7
- [18] Bingxin Ke, Anton Obukhov, Shengyu Huang, Nando Metzger, Rodrigo Caye Daudt, and Konrad Schindler. Repurposing diffusion-based image generators for monocular depth estimation. In *Proceedings of the IEEE/CVF conference on computer vision and pattern recognition*, pages 9492–9502, 2024. 3
- [19] Numair Khan, Min H Kim, and James Tompkin. Differentiable diffusion for dense depth estimation from multi-view images. In *Proceedings of the IEEE/CVF conference on computer vision and pattern recognition*, pages 8912–8921, 2021. 3
- [20] Moo Jin Kim, Karl Pertsch, Siddharth Karamcheti, Ted Xiao, Ashwin Balakrishna, Suraj Nair, Rafael Rafailov, Ethan Foster, Grace Lam, Pannag Sanketi, et al. Openvla: An open-source vision-language-action model. arXiv preprint arXiv:2406.09246, 2024. 2
- [21] Diederik P Kingma and Max Welling. Auto-encoding variational bayes. *arXiv preprint arXiv:1312.6114*, 2013. 3
- [22] Hang Lai, Jiahang Cao, Jiafeng Xu, Hongtao Wu, Yunfeng Lin, Tao Kong, Yong Yu, and Weinan Zhang. World model-based perception for visual legged locomotion. In 2025 IEEE International Conference on Robotics and Automation (ICRA), pages 11531–11537. IEEE, 2025. 3
- [23] Xinghang Li, Minghuan Liu, Hanbo Zhang, Cunjun Yu, Jie Xu, Hongtao Wu, Chilam Cheang, Ya Jing, Weinan Zhang, Huaping Liu, et al. Vision-language foundation models as effective robot imitators. *arXiv preprint arXiv:2311.01378*, 2023. 2
- [24] Xinhai Li, Jialin Li, Ziheng Zhang, Rui Zhang, Fan Jia, Tiancai Wang, Haoqiang Fan, Kuo-Kun Tseng, and Ruiping Wang. Robogsim: A real2sim2real robotic gaussian splatting simulator. *arXiv preprint arXiv:2411.11839*, 2024. 2
- [25] Haolin Liu, Chongjie Ye, Yinyu Nie, Yingfan He, and Xiaoguang Han. Lasa: Instance reconstruction from real scans using a large-scale aligned shape annotation dataset. In Proceedings of the IEEE/CVF Conference on Computer Vision and Pattern Recognition, pages 20454–20464, 2024. 3, 6
- [26] Minghuan Liu, Zixuan Chen, Xuxin Cheng, Yandong Ji, Ri-Zhao Qiu, Ruihan Yang, and Xiaolong Wang. Visual whole-body control for legged loco-manipulation. arXiv preprint arXiv:2403.16967, 2024. 2, 3
- [27] Minghuan Liu, Zhengbang Zhu, Xiaoshen Han, Peng Hu, Haotong Lin, Xinyao Li, Jingxiao Chen, Jiafeng Xu, Yichu Yang, Yunfeng Lin, Xinghang Li, Yong Yu, Weinan Zhang, Tao Kong, and Bingyi Kang. Manipulation as in simula-

- tion: Enabling accurate geometry perception in robots. *arXiv* preprint, 2025. 2, 3, 6
- [28] Ajay Mandlekar, Danfei Xu, Josiah Wong, Soroush Nasiriany, Chen Wang, Rohun Kulkarni, Li Fei-Fei, Silvio Savarese, Yuke Zhu, and Roberto Martín-Martín. What matters in learning from offline human demonstrations for robot manipulation. arXiv preprint arXiv:2108.03298, 2021. 2
- [29] Ajay Mandlekar, Soroush Nasiriany, Bowen Wen, Iretiayo Akinola, Yashraj Narang, Linxi Fan, Yuke Zhu, and Dieter Fox. Mimicgen: A data generation system for scalable robot learning using human demonstrations. In 7th Annual Conference on Robot Learning, 2023. 6
- [30] Bhairav Mehta, Manfred Diaz, Florian Golemo, Christopher J Pal, and Liam Paull. Active domain randomization. In Conference on Robot Learning, pages 1162–1176. PMLR, 2020. 8
- [31] Mingjie Pan, Jiyao Zhang, Tianshu Wu, Yinghao Zhao, Wenlong Gao, and Hao Dong. Omnimanip: Towards general robotic manipulation via object-centric interaction primitives as spatial constraints. In *Proceedings of the Computer Vision and Pattern Recognition Conference*, pages 17359–17369, 2025. 3
- [32] Xue Bin Peng, Marcin Andrychowicz, Wojciech Zaremba, and Pieter Abbeel. Sim-to-real transfer of robotic control with dynamics randomization. In 2018 IEEE international conference on robotics and automation (ICRA), pages 3803– 3810. IEEE, 2018. 3
- [33] Luigi Piccinelli, Yung-Hsu Yang, Christos Sakaridis, Mattia Segu, Siyuan Li, Luc Van Gool, and Fisher Yu. Unidepth: Universal monocular metric depth estimation. In *Proceedings of the IEEE/CVF Conference on Computer Vision and Pattern Recognition*, pages 10106–10116, 2024. 8
- [34] Robin Rombach, Andreas Blattmann, Dominik Lorenz, Patrick Esser, and Björn Ommer. High-resolution image synthesis with latent diffusion models. In *Proceedings of the IEEE/CVF conference on computer vision and pattern recognition*, pages 10684–10695, 2022. 3
- [35] Robin Rombach, Andreas Blattmann, Dominik Lorenz, Patrick Esser, and Bjorn Ommer. High-resolution image synthesis with latent diffusion models. In CVPR, 2022. 6, 7
- [36] Saurabh Saxena, Charles Herrmann, Junhwa Hur, Abhishek Kar, Mohammad Norouzi, Deqing Sun, and David J Fleet. The surprising effectiveness of diffusion models for optical flow and monocular depth estimation. *Advances in Neural Information Processing Systems*, 36:39443–39469, 2023. 3
- [37] Mingyo Seo, Steve Han, Kyutae Sim, Seung Hyeon Bang, Carlos Gonzalez, Luis Sentis, and Yuke Zhu. Deep imitation learning for humanoid loco-manipulation through human teleoperation. In 2023 IEEE-RAS 22nd International Conference on Humanoid Robots (Humanoids), pages 1–8. IEEE, 2023. 2
- [38] Yuan Shi, Huiyun Cao, Bin Xia, Rui Zhu, Qingmin Liao, and Wenming Yang. Dsr-diff: Depth map super-resolution with diffusion model. *Pattern Recognition Letters*, 184:225–231, 2024. 3
- [39] Jiaming Song, Chenlin Meng, and Stefano Ermon. Denoising diffusion implicit models. In *International Conference on Learning Representations*, 2021. 2, 3

- [40] Nitish Sontakke, Hosik Chae, Sangjoon Lee, Tianle Huang, Dennis W Hong, and Sehoon Hal. Residual physics learning and system identification for sim-to-real transfer of policies on buoyancy assisted legged robots. In 2023 IEEE/RSJ International Conference on Intelligent Robots and Systems (IROS), pages 392–399. IEEE, 2023. 3
- [41] Hiromu Taketsugu, Takeru Oba, Takahiro Maeda, Shohei Nobuhara, and Norimichi Ukita. Physical plausibility-aware trajectory prediction via locomotion embodiment. In *Proceedings of the Computer Vision and Pattern Recognition Conference*, pages 12324–12334, 2025. 3
- [42] Josh Tobin, Rachel Fong, Alex Ray, Jonas Schneider, Wojciech Zaremba, and Pieter Abbeel. Domain randomization for transferring deep neural networks from simulation to the real world. In 2017 IEEE/RSJ international conference on intelligent robots and systems (IROS), pages 23–30. IEEE, 2017. 3
- [43] Albert Tung, Josiah Wong, Ajay Mandlekar, Roberto Martín-Martín, Yuke Zhu, Li Fei-Fei, and Silvio Savarese. Learning multi-arm manipulation through collaborative teleoperation. In 2021 IEEE International Conference on Robotics and Automation (ICRA), pages 9212–9219. IEEE, 2021. 2
- [44] Chenxi Wang, Hongjie Fang, Hao-Shu Fang, and Cewu Lu. Rise: 3d perception makes real-world robot imitation simple and effective. In 2024 IEEE/RSJ International Conference on Intelligent Robots and Systems (IROS), pages 2870–2877. IEEE, 2024. 6, 7, 8
- [45] Jun Wang, Yuzhe Qin, Kaiming Kuang, Yigit Korkmaz, Akhilan Gurumoorthy, Hao Su, and Xiaolong Wang. Cyberdemo: Augmenting simulated human demonstration for real-world dexterous manipulation. In *Proceedings of the IEEE/CVF Conference on Computer Vision and Pattern Recognition*, pages 17952–17963, 2024. 3
- [46] Zhen Wang, Qiangeng Xu, Feitong Tan, Menglei Chai, Shichen Liu, Rohit Pandey, Sean Fanello, Achuta Kadambi, and Yinda Zhang. Mvdd: Multi-view depth diffusion models. In *European Conference on Computer Vision*, pages 236–253. Springer, 2024. 3
- [47] Hongtao Wu, Ya Jing, Chilam Cheang, Guangzeng Chen, Jiafeng Xu, Xinghang Li, Minghuan Liu, Hang Li, and Tao Kong. Unleashing large-scale video generative pretraining for visual robot manipulation. *arXiv preprint arXiv:2312.13139*, 2023. 2
- [48] Shangning Xia, Hongjie Fang, Cewu Lu, and Hao-Shu Fang. Cage: Causal attention enables data-efficient generalizable robotic manipulation. In 2025 IEEE International Conference on Robotics and Automation (ICRA), pages 13242– 13249. IEEE, 2025. 7, 8
- [49] Fanbo Xiang, Yuzhe Qin, Kaichun Mo, Yikuan Xia, Hao Zhu, Fangchen Liu, Minghua Liu, Hanxiao Jiang, Yifu Yuan, He Wang, et al. Sapien: A simulated part-based interactive environment. In *Proceedings of the IEEE/CVF conference on computer vision and pattern recognition*, pages 11097–11107, 2020. 3
- [50] Mutian Xu, Chongjie Ye, Haolin Liu, Yushuang Wu, Jiahao Chang, and Xiaoguang Han. Stable-sim2real: Exploring simulation of real-captured 3d data with two-stage depth dif-

- fusion. In *Proceedings of the IEEE/CVF International Conference on Computer Vision*, pages 2609–2619, 2025. 2, 3
- [51] Lihe Yang, Bingyi Kang, Zilong Huang, Zhen Zhao, Xiao-gang Xu, Jiashi Feng, and Hengshuang Zhao. Depth anything v2. arXiv:2406.09414, 2024. 8
- [52] Yanjie Ze, Zixuan Chen, Wenhao Wang, Tianyi Chen, Xialin He, Ying Yuan, Xue Bin Peng, and Jiajun Wu. Generalizable humanoid manipulation with 3d diffusion policies. arXiv preprint arXiv:2410.10803, 2024. 2
- [53] Yanjie Ze, Gu Zhang, Kangning Zhang, Chenyuan Hu, Muhan Wang, and Huazhe Xu. 3d diffusion policy: Generalizable visuomotor policy learning via simple 3d representations. In *Proceedings of Robotics: Science and Systems* (RSS), 2024. 6
- [54] Yanjie Ze, Gu Zhang, Kangning Zhang, Chenyuan Hu, Muhan Wang, and Huazhe Xu. 3d diffusion policy: Generalizable visuomotor policy learning via simple 3d representations. arXiv preprint arXiv:2403.03954, 2024. 2
- [55] Lvmin Zhang, Anyi Rao, and Maneesh Agrawala. Adding conditional control to text-to-image diffusion models, 2023. 6, 7
- [56] Xiang Zhang, Bingxin Ke, Hayko Riemenschneider, Nando Metzger, Anton Obukhov, Markus Gross, Konrad Schindler, and Christopher Schroers. Betterdepth: Plug-and-play diffusion refiner for zero-shot monocular depth estimation. Advances in Neural Information Processing Systems, 37: 108674–108709, 2024. 3
- [57] Tony Z Zhao, Vikash Kumar, Sergey Levine, and Chelsea Finn. Learning fine-grained bimanual manipulation with low-cost hardware. arXiv preprint arXiv:2304.13705, 2023.
- [58] Haoyi Zhu, Yating Wang, Di Huang, Weicai Ye, Wanli Ouyang, and Tong He. Point cloud matters: Rethinking the impact of different observation spaces on robot learning. Advances in Neural Information Processing Systems, 37:77799–77830, 2024. 2
- [59] Ziwen Zhuang, Zipeng Fu, Jianren Wang, Christopher Atkeson, Soeren Schwertfeger, Chelsea Finn, and Hang Zhao. Robot parkour learning. arXiv preprint arXiv:2309.05665, 2023. 3
- [60] Ziwen Zhuang, Shenzhe Yao, and Hang Zhao. Humanoid parkour learning. arXiv preprint arXiv:2406.10759, 2024. 3